

## NUMERICAL SIMULATION OF FLOW OVER NACA-0012 AIRFOIL PITCHING AT LOW FREQUENCIES

Aasha G C

Vishal Raj

Rohan Srikanth

Ajit H A

Department of Mechanical Engineering

B. M. S. College of Engineering

Bengaluru, India

Advisors:

Ramesh Kolluru, CFD Lab, Department of Aerospace Engineering, IISc

Ramesh. M. Chalkapure, Assistant Professor, Department of Mechanical  
Engineering, BMCSE

# OUTLINE

- 1 MOTIVATION
- 2 PROBLEM DEFINITION
- 3 SU2: MODELING
- 4 SU2: NUMERICS
- 5 SU2: GEOMETRY AND MESH
- 6 SU2: GRID AND TIME INDEPENDENCE STUDY
- 7 OPENFOAM: SOLVER SETUP
- 8 RESULTS
- 9 CONCLUSION

# MOTIVATION

- Numerous aerospace and underwater vehicles and their components undergo oscillatory motion.
- Submarines, Autonomous Underwater Vehicles (AUVs), remotely operated underwater vehicles (ROVs) and their components when moving in shallow water.
- Flow of fluid is relative to low frequency oscillatory component.
- Such a flow can be considered to be quasi-steady in nature.
- Flow at low speed approaching the airfoil is incompressible.

## OBJECTIVES

- Numerical analysis over pitching NACA 0012.
- Open-source CFD platform SU2 and OpenFOAM for numerical analysis.
- Comparison of results obtained from both the software.

## PROBLEM DEFINITION

The following criteria outline the premise of the present study:

- Sinusoidal pitching motion of airfoil is:

$$\alpha(t) = \alpha_0 + \alpha_a \sin \omega t \quad (1)$$

- $\alpha_0 = 0^\circ$ ,  $\alpha_a = 9^\circ$ ,  $\omega = 0.15707 \frac{\text{rad}}{\text{sec}}$ .
- Static simulations are done for  $-9^\circ$ ,  $-7^\circ$ ,  $-5^\circ$ ,  $-2^\circ$ ,  $0^\circ$ ,  $2^\circ$ ,  $5^\circ$ ,  $7^\circ$  and  $9^\circ$  angles of attack (AOA).

TABLE: Flow parameters

S.N.	Parameters	Value/s
1	Velocity (U)	$30 \text{ ms}^{-1}$
2	Chord (c)	$0.15 \text{ m}$
3	Temperature (T)	$298 \text{ K}$
4	Reynolds number (Re)	$2.9\text{e}5$

- Incompressible RANS solver INC\_RANS is used in SU2 and PimpleFOAM in OpenFOAM.
- Turbulence modeling using Menter's SST model.
- Aerodynamic coefficients, like drag and lift coefficient, are analysed.
- Grid independence study is carried out.
- Static and dynamic simulation results from both SU2 and OpenFOAM are compared for various AoA.

# GOVERNING EQUATIONS

- Incompressible Navier Stokes governing equation:

$$\partial_t V + \nabla \cdot \bar{F}^c(V) - \nabla \cdot \bar{F}^v(V, \nabla V) = Q \quad (2)$$

in the domain  $\Omega$  for  $t < 0$ . [1]

$V$	Vector of working variables	$\{\rho, \bar{v}, T\}^T$
$\bar{F}^c(V)$	Vector of convective fluxes	$0.15 \bar{F}^c(V)$
$\bar{F}^v(V)$	vector of viscous fluxes	$\{., \bar{\tau}, \kappa \nabla T\}^T$
$Q$	Source term	absent

- Pressure-velocity coupling is realised through Chorin's artificial compressibility [2]:

$$\begin{aligned} \partial_t u_i + R \partial_j (u_i u_j) &= -\partial_i p + \Delta u_i + F_i, \\ \partial_t \rho + \partial_j u_j &= 0, P = \rho \end{aligned} \quad (3)$$

- Density model: CONSTANT DENSITY.

# TURBULENCE MODEL

- Viscosity( $\mu$ ) is dissolved into dynamic( $\mu_d$ ) and turbulent ( $\mu_t$ ) components as  $\mu = \mu_d + \mu_t$ . [3]
- $\mu_d$  is constant (a constant temperature flow analysis).
- $\mu_t$  is computed using the Menter's Shear Stress Transport (SST) Model [4] as:

$$\mu_t = \frac{\rho a_1 k}{\max(a_1 \omega, SF_2)} \quad (4)$$

- Menter's SST is a two-equation eddy-viscosity turbulence Model;

$$\begin{aligned} \frac{\partial k}{\partial t} + \frac{\partial(\rho U_i \omega)}{\partial x_i} &= \vec{P}_k - \beta^* \rho k \omega + \frac{\partial}{\partial x_i} \left[ (\mu + \sigma_k \mu_t) \frac{\partial k}{\partial x_i} \right] \\ \frac{\partial(\rho \omega)}{\partial t} + \frac{\partial(\rho U_i \omega)}{\partial x_i} &= \alpha \rho S^2 - \beta \rho \omega^2 + \left[ (\mu + \sigma_\omega \mu_t) \frac{\partial \omega}{\partial x_i} \right] + 2(1 - F_1) \rho \sigma_{\omega^2} \frac{1}{\omega} \frac{\partial k}{\partial x_i} \frac{\partial \omega}{\partial x_i} \end{aligned} \quad (5)$$

- It overcomes the sensitivity of  $k - \omega$  model to the values of  $\omega$ .
- Has better boundary layer modeling capabilities.

# SPACE INTEGRATION

- Convective flux vectors are averaged on faces of median-dual control volume from values at nodes on either side of the faces.[5]
- Flux Difference Splitting (FDS) scheme is used for the integration of convective fluxes.
- Monotone Upstream-centered Scheme for Conservation Laws (MUSCL) approach is used to achieve second-order accuracy.

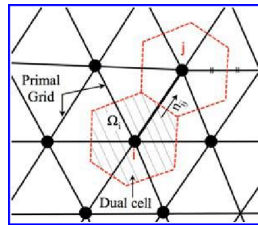


FIGURE: Schematic of the primal mesh and the control volume on a dual mesh [5]

- Viscous fluxes and their gradients are calculated using Green-Gauss method.
- The Green-Gauss method is observed to outperform the least-squares (LS) gradient method in the simulation of aerodynamic boundary layer flows over curved surfaces [6].

# TIME INTEGRATION

## Static Analysis Case

- Implicit Euler Scheme is used to discretize the system.
- Local-time-stepping is used to accelerate the convergence to a steady state.
- The option ITER is used to control the number of iterations.

## Dynamic Analysis Case

- To enable a time-dependent simulation the TIME\_DOMAIN option is set to YES.
- DUAL\_TIME\_STEPPING-2ND\_ORDER is selected which solves the following problem:

$$\frac{\partial V}{\partial \tau} + R^* V = 0, \quad (6)$$

where  $R^* V = \frac{3}{2t} V + \frac{1}{|\Omega|^{n+1}} (R(V) - \frac{2}{t} V^n |\Omega|^n + \frac{1}{2t} V^{n-1} |\Omega|^{n-1})$  is the residual of the governing equation for real time  $t$  and fictitious time  $\tau$  [5].

- The unsteady problem is transformed into a steady problem at each physical time step.
- The options TIME\_ITER or MAX\_TIME are used to control the number of physical time iterations.

# LINEAR SOLVER AND PRECONDITIONER

## Linear Solver

- Flexible Generalised Minimum Residual (FGMRES) is the linear solver chosen.
- FGMRES is a more "flexible" and faster version of the GMRES.
- It is a Krylov-space iterative solver capable of handling non-symmetric matrices.
- It has an inner iteration that uses GMRES to precondition the system, and an outer iteration that minimizes the system residual to generate the solution.[7]

## Preconditioner

- Linelet preconditioner is used for the preconditioning the matrix.
- It improves the convergence rate of the Krylov subspace linear solvers. [5]
- It can reduce the number of preconditioning conjugate gradient (PCG) iterations for meshes with highly stretched elements. [8]

# GEOMETRY

- 2D C-grid structured mesh.
- SU2\_DEF function is applied to reduce the unit chord of the original mesh to 0.15m.
- The grid is stretched in the direction normal to wall.

Marker	Boundary Condition
airfoil	Constant heatflux
farfield	Farfield

- Constant heatflux boundary condition to enforce the adiabatic no-slip wall condition on the airfoil.
- Farfield boundary condition to enforce free-stream values on the farfield.

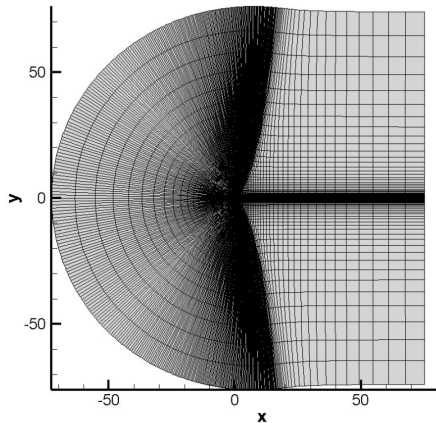


FIGURE: C grid structured mesh for NACA 0012

Farfield Ex- tension	Overall Points	Points on the airfoil
500c	57824	256

# MESH MOVEMENT

- The volumetric deformation procedure is used for moving the mesh.
- DEFORMATION value is applied through the option SURFACE\_MOVEMENT.
- The surface boundary (airfoil) is moved, followed by deformation of the volume mesh.

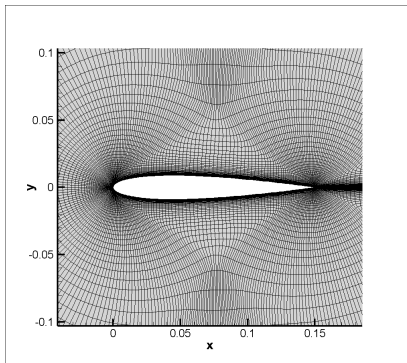


FIGURE: Mesh at 0° AOA

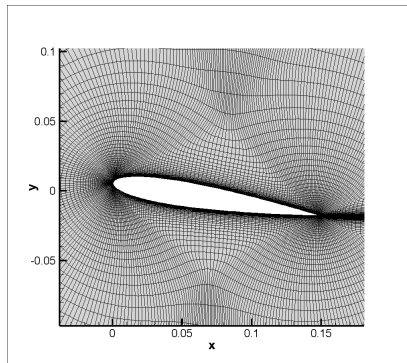


FIGURE: Mesh at 9° AOA

## GRID INDEPENDENT STUDY

- A grid independence study was carried out on the grids:
  - 1  $255 \times 65$
  - 2  $449 \times 129$
  - 3  $897 \times 257$
- The mesh description and the corresponding coefficient of lift (Cl) and coefficient of drag (Cd) are tabulated.

TABLE: Cl and Cd at  $9^\circ$  AOA for mesh 1, 2, and 3

Mesh No.	Mesh	Cl	Cd
1	$255 \times 65$	0.882913	0.028536
2	$449 \times 129$	0.890099	0.022138
3	$897 \times 257$	0.892554	0.020597

- Cl values did not show any significant change with increase in grid refineness.
- Cd values for Mesh 2 and 3 were significantly close.

# TIME INDEPENDENT STUDY

- Time Independence study was conducted over the course of a half-cycle with three sample step sizes of 0.25s, 0.11s and 0.05s.
- The CI curves for all the three cases showed perfect agreement with each other.
- The Cd plots overlapped for most of the duration with only  $\Delta t = 0.05$  showing slight deviations.

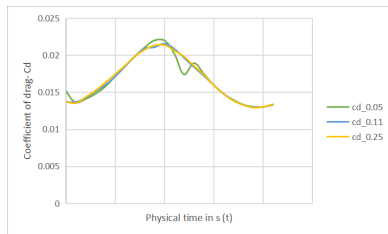


FIGURE: Cd vs t (SU2)

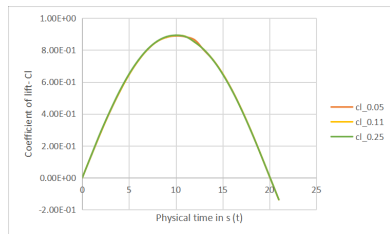


FIGURE: Cl vs t (SU2)

# SOLVERS AND METHODOLOGY: OPENFOAM

## STATIC CASE ANALYSIS

- Static analysis is executed with the solver - PISOFOAM, is strictly an in-compressible flow solver, coupling between density and pressure is removed, as well as the coupling between the energy equation.
- It is used to simulate transient cases, with an allowance of higher than 1 Courant number.
- PISO operator works on the basis of outer and inner correctors. The number of outer correctors defines how many "outer iterations" is to be performed, which is equivalent to the number of times the system of equations are computed. [9]
- The inner correctors determine the number of iterations required to compute the pressure field.

# SOLVERS AND METHODOLOGY: OPENFOAM

## DYNAMIC CASE ANALYSIS

- The PIMPLE algorithm is used to solve incompressible, transient cases in OpenFOAM, with dynamic mesh capabilities. It solves the continuity and momentum equations, which are the constrained equations of incompressible navier-stokes equation.

$$\nabla \cdot U = 0$$

and the momentum equation:

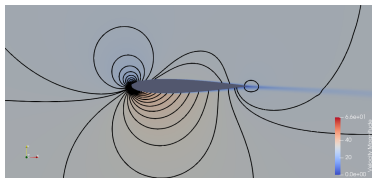
$$\frac{\partial u}{\partial t} + (u \cdot \nabla)u = \nu \nabla^2 u - \nabla p + g$$

- The PIMPLE algorithm can be considered as a SIMPLE algorithm for every time step, where "outer correctors" are the iterations, and once converged will move on to the next time step.
- For the dynamic mesh-morphing mechanism, 'displacementLaplacian' uses the mesh methodology known as dynamicMotionSolverFvMesh, which is used in cases where the motion of interval mesh points are solved for using boundary conditions and diffusivity.

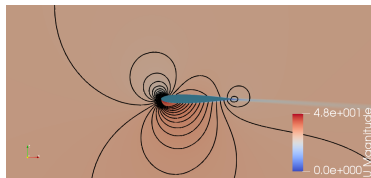
# STATIC ANALYSIS CASE

## VELOCITY CONTOURS

- The velocity contours from both the software are observed to be very similar.
- The maximum value is slightly higher for SU2.

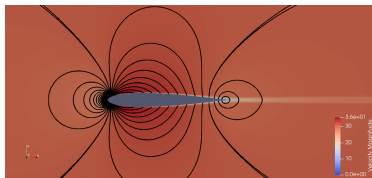


(A) SU2

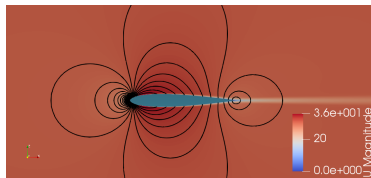


(B) OpenFOAM

FIGURE: Velocity Contours at  $-5^\circ$  AOA



(A) SU2



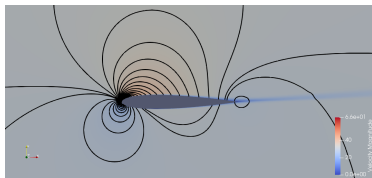
(B) OpenFOAM

FIGURE: Velocity Contours at  $0^\circ$  AOA

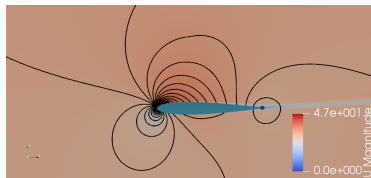
# STATIC ANALYSIS CASE

## VELOCITY CONTOURS CONTINUED

- A thin trail of relatively lower velocity is observed beyond airfoil.
- Flow velocity around the leading edge increases as AOA increases.

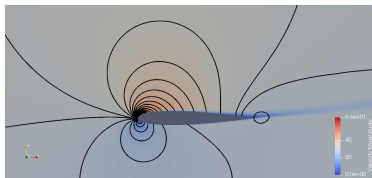


(A) SU2

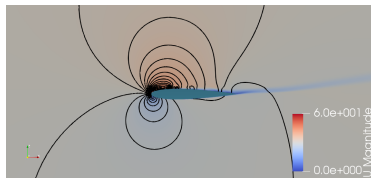


(B) OpenFOAM

FIGURE: Velocity Contours at 5° AOA



(A) SU2



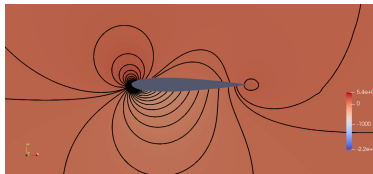
(B) OpenFOAM

FIGURE: Velocity Contours at 9° AOA

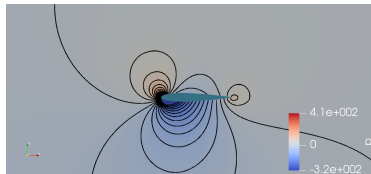
# STATIC ANALYSIS CASE

## PRESSURE CONTOURS

- Flow is attached for SU2 all throughout the studied range of angles.
- Flow is observed to separate at AOA 9 for OpenFOAM.

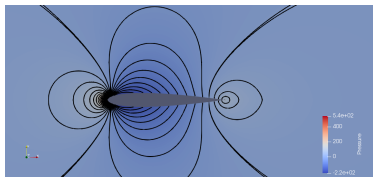


(A) SU2

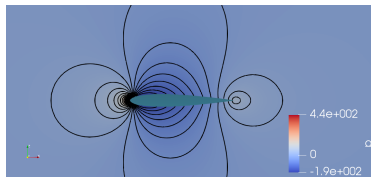


(B) OpenFOAM

FIGURE: Pressure Contours at -5° AOA



(A) SU2

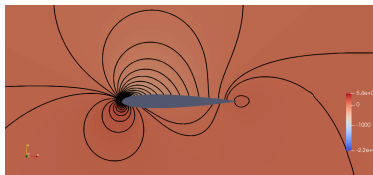


(B) OpenFOAM

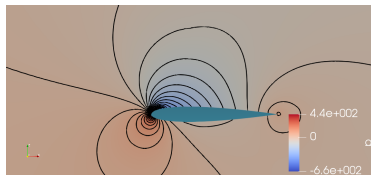
FIGURE: Pressure Contours at 0° AOA

# STATIC ANALYSIS CASE

## PRESSURE CONTOURS CONTINUED

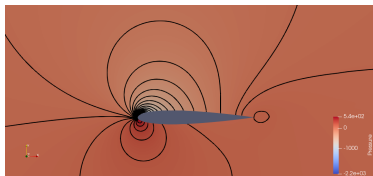


(A) SU2

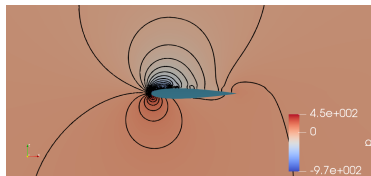


(B) OpenFOAM

FIGURE: Pressure Contours at 5° AOA



(A) SU2

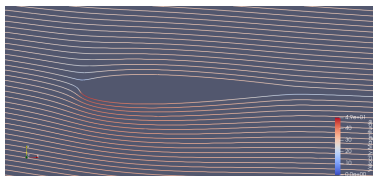


(B) OpenFOAM

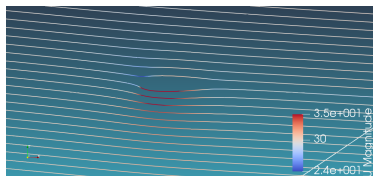
FIGURE: Pressure Contours at 9° AOA

# STATIC ANALYSIS CASE

## STREAMLINES

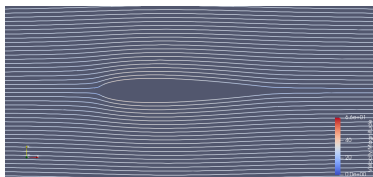


(A) SU2

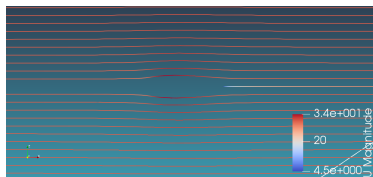


(B) OpenFOAM

FIGURE: Streamlines at -5° AOA



(A) SU2

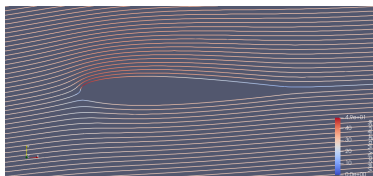


(B) OpenFOAM

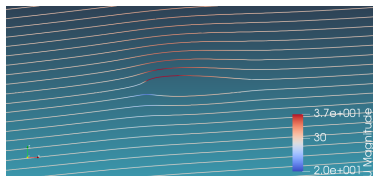
FIGURE: Streamlines at 0° AOA

# STATIC ANALYSIS CASE

STREAMLINES CONTINUED

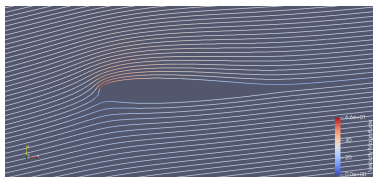


(A) SU2

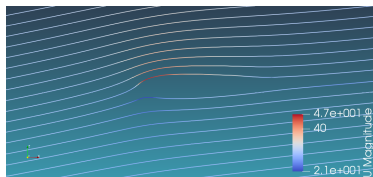


(B) OpenFOAM

FIGURE: Streamlines at 5° AOA



(A) SU2



(B) OpenFOAM

FIGURE: Streamlines at 9° AOA

# STATIC ANALYSIS CASE

## FLOW COEFFICIENTS

- Coefficient of lift (Cl) curves are observed to be linear.
- Coefficient of drag (Cd) is seen to be the least at zero angle of incidence.
- Cd increases for higher AOA due to increase in resistance to flow offered by the airfoil.
- Cl and Cd obtained from both the software are seen to be in good agreement with each other.

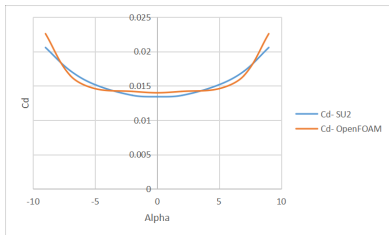


FIGURE: Cd vs alpha

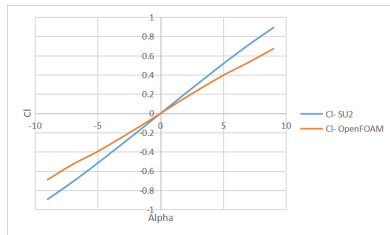
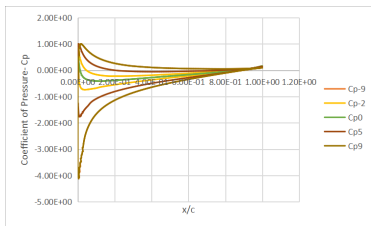


FIGURE: Cl vs alpha

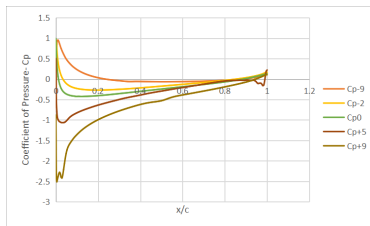
# STATIC ANALYSIS CASE

## PRESSURE COEFFICIENT

- Coefficient of pressure ( $C_p$ ) curve along the chord line is seen to be smooth.
- This can be attributed to the absence of boundary layer turbulence.
- The minimum value of  $C_p$  is observed to be lesser for OpenFOAM.
- This is caused by the earlier onset of leading edge vortices (LEV) at around  $9^\circ$  AOA, and is shed as the AOA increases.



(A) SU2



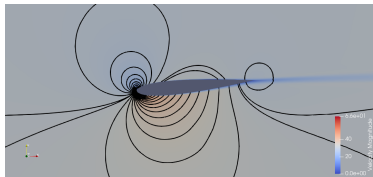
(B) OpenFOAM

FIGURE:  $C_p$  vs  $x/c$

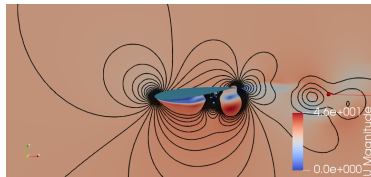
# DYNAMIC ANALYSIS CASE

## VELOCITY CONTOUR

- Velocity contours for dynamic case in SU2 are similar to the static case.
- Flow is still attached throughout the airfoil surface.

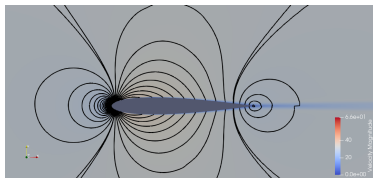


(A) SU2

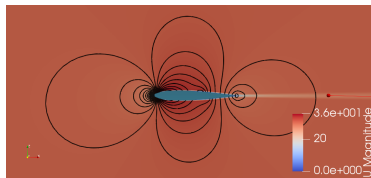


(B) OpenFOAM

FIGURE: Velocity Contours at  $-5^\circ$  AOA



(A) SU2



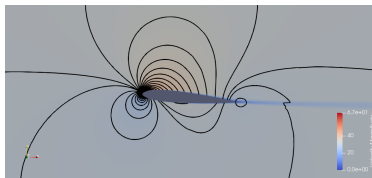
(B) OpenFOAM

FIGURE: Velocity Contours at  $0^\circ$  AOA

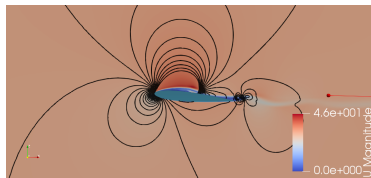
# DYNAMIC ANALYSIS CASE

## VELOCITY CONTOUR CONTINUED

- Boundary layer turbulence is seen to develop around angles as low as 5 AOA for OpenFOAM.
- Fully developed vortices are shed at the trailing edge downstream for higher angles (around 9 AOA).

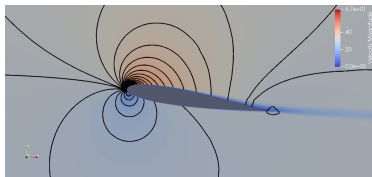


(A) SU2

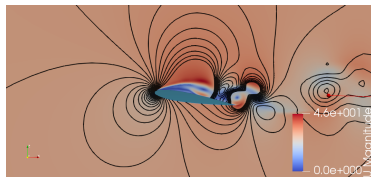


(B) OpenFOAM

FIGURE: Velocity Contours at 5° AOA



(A) SU2



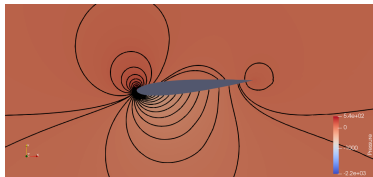
(B) OpenFOAM

FIGURE: Velocity Contours at 9° AOA

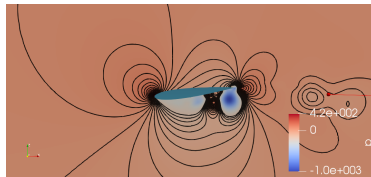
# DYNAMIC ANALYSIS CASE

## PRESSURE CONTOUR

- The pressure contours for dynamic case in SU2 are similar to the static case.
- The flow is still attached throughout the airfoil surface.

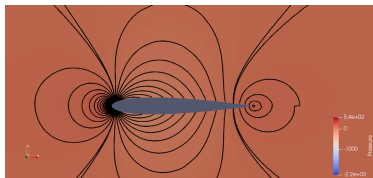


(A) SU2

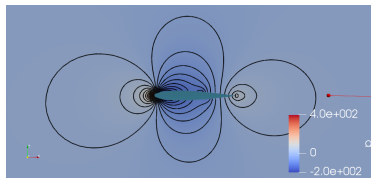


(B) OpenFOAM

FIGURE: Pressure Contours at  $-5^\circ$  AOA



(A) SU2



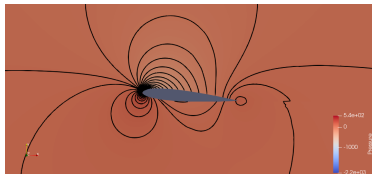
(B) OpenFOAM

FIGURE: Pressure Contours at  $0^\circ$  AOA

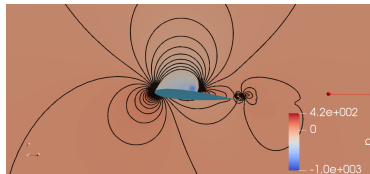
# DYNAMIC ANALYSIS CASE

## PRESSURE CONTOUR CONTINUED

- Boundary layer formation is prominent and thicker than that observed in SU2.
- A prominent lower pressure zone develops on the leeward side as the AOA increases.

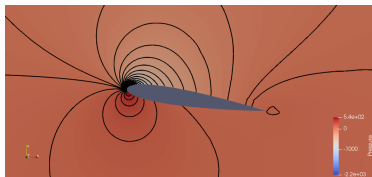


(A) SU2

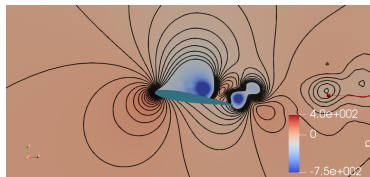


(B) OpenFOAM

FIGURE: Pressure Contours at 5° AOA



(A) SU2

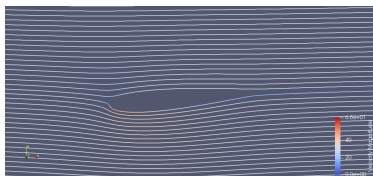


(B) OpenFOAM

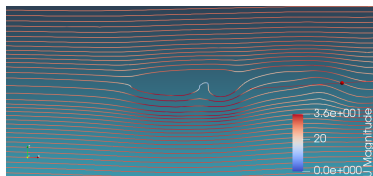
FIGURE: Pressure Contours at 9° AOA

## DYNAMIC ANALYSIS CASE

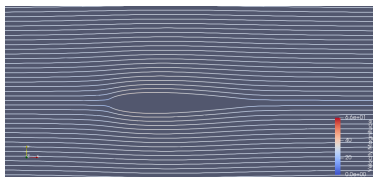
## STREAMLINES



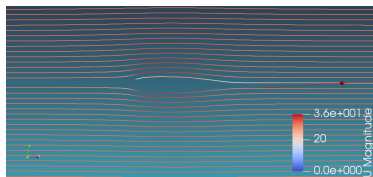
(A) SU2



(B) OpenFOAM

FIGURE: Streamlines at  $-5^\circ$  AOA

(A) SU2

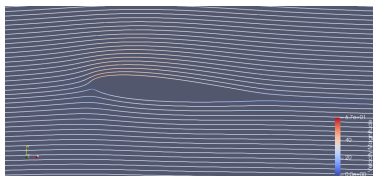


(B) OpenFOAM

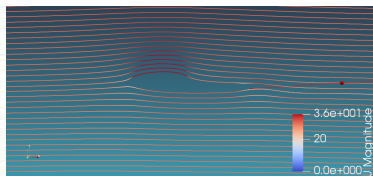
FIGURE: Streamlines at  $0^\circ$  AOA

## DYNAMIC ANALYSIS CASE

STREAMLINES CONTINUED

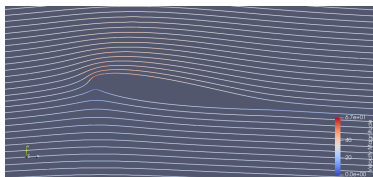


(A) SU2

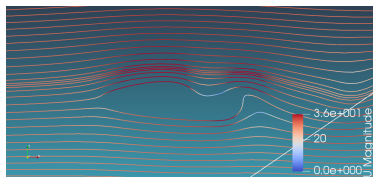


(B) OpenFOAM

FIGURE: Streamlines at 5° AOA



(A) SU2



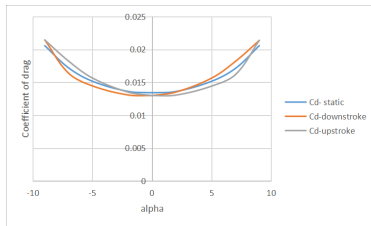
(B) OpenFOAM

FIGURE: Streamlines at 9° AOA

# DYNAMIC ANALYSIS CASE

## COEFFICIENT OF DRAG

- The nature of the curve for dynamic case is similar to static.
- Minor fluctuations are observed during downstroke (trailing edge pitching down) for SU2.
- These fluctuations subside gradually and a smooth periodic pattern develops over time.
- Cd obtained from OpenFOAM shows a significantly higher range, with prominent fluctuations for negative AOA.



(A) SU2

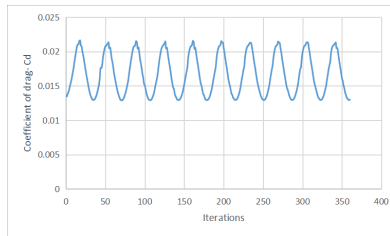
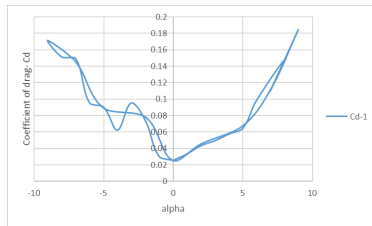


FIGURE: Time-dependent coefficient of drag- Cd



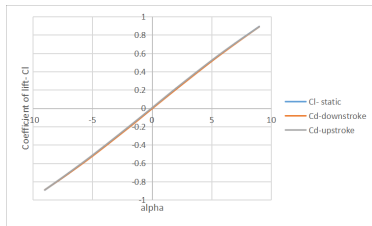
(B) OpenFOAM

FIGURE: Cd vs alpha

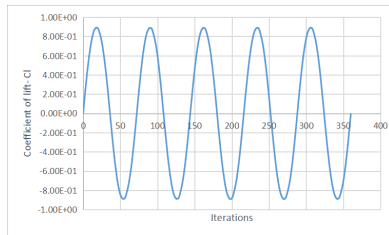
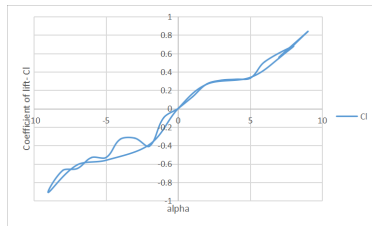
# DYNAMIC ANALYSIS CASE

## COEFFICIENT OF LIFT

- Both static and dynamic  $C_l$  values are similar for SU2.
- Hysteresis effects are negligible, as there is no sign of dynamic stalling.
- A stable periodic pattern develops over the course of few cycles.
- Fluctuations are observed in case of OpenFOAM, especially during downstroke motion in the negative AOA region, due to lesser cycles being considered and mesh refinement.



(A) SU2

FIGURE: Time-dependent coefficient of lift-  $C_l$ 

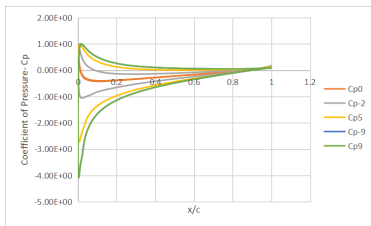
(B) OpenFOAM

FIGURE:  $C_l$  vs  $\alpha$

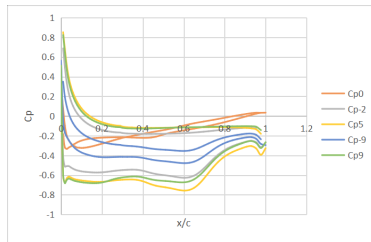
# DYNAMIC ANALYSIS CASE

## PRESSURE COEFFICIENT

- The nature of the curve for dynamic case in SU2 is similar to the static case.
- The magnitude of the minimum value of  $C_p$  is lesser for lower magnitude of AOA for dynamic flow.
- Due to the presence of wakes and pressure disturbances for OpenFOAM,  $C_p$  curve flattens.
- The fluctuations observed become more prominent with increasing AOA.



(A) SU2



(B) OpenFOAM

FIGURE:  $C_p$  vs  $x/c$

# OUTPUT

- Presence of turbulence in the flow leads to dissipation of energy.
- This dissipation of energy reduces the range of pressure values in the domain.
- $C_p$  min is observed lower for SU2, the difference increases with increasing AOA.
- This can be attributed to the presence of wakes and vortices in OpenFOAM, at higher angles, increasing the pressure drag to significant amount and hence increasing the pressure. (Magnitude)

TABLE: Output for Static Case

AOA	Cd SU2	Cd OpenFOAM	Cl SU2	Cl OpenFOAM	Cp min SU2	Cp min OpenFOAM
-2	0.0136	0.0142	-0.209	-0.163	-0.74	-0.62
5	0.0152	0.0146	0.516	0.401	-1.77	-1.14
9	0.0206	0.0226	0.893	0.679	-4.12	-2.6

TABLE: Output for Dynamic Case

AOA	Cd SU2	Cd OpenFOAM	Cl SU2	Cl OpenFOAM	Cp min SU2	Cp min OpenFOAM
-2	0.013	0.074	-0.216	-0.408	-0.2	-0.61
5	0.016	0.067	0.512	0.37	-1.75	-1.2
9	0.021	0.184	0.889	0.84	-4.06	-1.7

# CONCLUSION

- With the nature of pitching being quasi-steady, the static and dynamic results are observed to bear good resemblance.
- The flow and flow parameters quickly develop a steady periodic pattern over the course of a few cycles.
- The major difference emerging between SU2 and OpenFOAM is in the  $C_d$  values, which are higher for OpenFOAM by 0.16.
- This could be attributed to more extensive presence of boundary layer turbulence, and kinetic energy of the fluid which in turn gives rise to wakes and trailing edge vortices at higher AOA.
- A possible explanation for such a flow-field could be the insufficient grid resolution in OpenFOAM, as a trial simulation on a finer mesh was observed to give lower values of  $C_d$ .
- As the OpenFOAM results are from the first pitching cycle, the flow is suspected to be transient and further analysis over a large number of cycles is expected to reduce the values of flow-coefficients.
- In conclusion, for a low frequency pitching under quasi steady conditions, the static and dynamic cases are found to be similar.

## FUTURE WORK

- The differences observed in the dynamic results between the software could be associated with the respective modelling techniques and solver algorithms, which shall be explored further.
- An experimental validation to be conducted in the future would provide better insights on the flow physics involved in a low frequency pitching motion.

## REFERENCES



su2foundation, "Guide to version v7."



A. J. Chorin, "A numerical method for solving incompressible viscous flow problems," *Journal of computational physics*, vol. 2, no. 1, pp. 12–26, 1967.



T. D. Economou, "Simulation and adjoint-based design for variable density incompressible flows with heat transfer," *AIAA Journal*, pp. 1–13, 2019.



F. R. Menter, M. Kuntz, and R. Langtry, "Ten years of industrial experience with the sst turbulence model," *Turbulence, heat and mass transfer*, vol. 4, no. 1, pp. 625–632, 2003.



F. Palacios, J. Alonso, *et al.*, "Stanford university unstructured (su 2): An open-source integrated computational environment for multi-physics simulation and design," in *51st AIAA aerospace sciences meeting including the new horizons forum and aerospace exposition*, p. 287.



A. Syrakos, S. Varchanis, *et al.*, "A critical analysis of some popular methods for the discretisation of the gradient operator in finite volume methods," *Physics of Fluids*, vol. 29, no. 12, p. 127103, 2017.



B. DeVries *et al.*, "Parallel implementations of fgmres for solving large, sparse non-symmetric linear systems," *Procedia Computer Science*, vol. 18, pp. 491–500, 2013.



O. Soto, R. Löhner, and F. Camelli, "A linelet preconditioner for incompressible flow solvers," *International Journal of Numerical Methods for Heat & Fluid Flow*, 2003.



"Simscale," 2012.

Thank You